ORIGINAL ARTICLE

Corrosion behaviours of the dental magnetic keeper complexes made by different alloys and methods

Min-Ke Wu[1], Ning Song[1], Fei Liu[1], Liang Kou[2], Xiao-Wen Lu[2], Min Wang[1], Hang Wang[1] and Jie-Fei Shen[1]

The keeper and cast dowel–coping, as a primary component for a magnetic attachment, is easily subjected to corrosion in a wet environment, such as the oral cavity, which contains electrolyte-rich saliva, complex microflora and chewing behaviour and so on. The objective of this *in vitro* study was to examine the corrosion resistance of a dowel and coping-keeper complex fabricated by finish keeper and three alloys (cobalt–chromium, CoCr; silver–palladium–gold, PdAu; gold–platinum, AuPt) using a laser-welding process and a casting technique. The surface morphology characteristics and microstructures of the samples were examined by means of metallographic microscope and scanning electron microscope (SEM). Energy-dispersive spectroscopy (EDS) with SEM provided elements analysis information for the test samples after 10% oxalic acid solution etching test. Tafel polarization curve recordings demonstrated parameter values indicating corrosion of the samples when subjected to electrochemical testing. This study has suggested that massive oxides are attached to the surface of the CoCr–keeper complex but not to the AuPt–keeper complex. Only the keeper area of cast CoCr–keeper complex displayed obvious intergranular corrosion and changes in the Fe and Co elements. Both cast and laser-welded AuPt–keeper complexes had the highest free corrosion potential, followed by the PdAu–keeper complex. We concluded that although the corrosion resistance of the CoCr–keeper complex was worst, the keeper surface passive film was actually preserved to its maximum extent. The laser-welded CoCr– and PdAu–keeper complexes possessed superior corrosion resistance as compared with their cast specimens, but no significant difference was found between the cast and laser-welded AuPt–keeper complexes. The Fe-poor and Cr-rich band, appearing on the edge of the keeper when casting, has been proven to be a corrosion-prone area.

INTRODUCTION

Dental magnetic attachment provides retention for removable dental prostheses by creating a magnetic force between a magnet and a keeper.[1–10] The core of the magnet is made of rare-earth alloy and encapsulated by a stainless steel yoke for providing protection.[5,11–12] It is placed onto the tissue side of the denture according to the position of the keeper. The keeper could be placed into a metal post-core supported by an endodontically treated root. It could also be attached to the metal framework of a fixed dental prosthesis. Therefore, because the keeper and cast dowel-coping create a complex, we named it the keeper complex in this study. The dowel and coping could be made from common dental alloys such as cobalt–chromium (CoCr) alloy, silver–palladium–gold (PdAu) alloy and gold–platinum (AuPt) alloy. The keeper could be cast or laser-welded into a dowel and coping as described in our previous study.[13]

Since the keeper complex is constantly subjected to the oral environment, which contains electrolyte-rich saliva, complex micro-

bial flora, and is subject to chewing behaviour, its ability to withstand corrosion, such as tarnish, rust, peeling and cracking, is a key factor in the overall survival rate of a dental magnetic attachment system.[14–15] Previous corrosion studies on dental magnetic attachments have focused on the magnet and its rare-earth alloy core,[12,16–19] even when it is sealed with excellent corrosion resistance materials by laser welding.[20] However, little has been reported on the keeper or the keeper complex. Thus, it is critical to explore the corrosion resistance of the complex due to its long-term fixation in the oral cavity.

Generally, there are two types of corrosion reactions: non-electrochemical corrosion and electrochemical corrosion, with the latter being of more significance in a wet conductive environment such as the oral cavity due to its galvanic effect.[21] Metal in isolated use shows a slow rate of electrochemical corrosion but accelerates when coupled.[22–23] The keeper complex usually consists of two different metals by diverse fabrication methods such as casting and laser-welding processes. The relevant factors related to the corrosion of

dental metal materials include their types, components, craftsmanship and more,[13,24–26] all of which could have an influence on their original characteristics.

In this study, we first proposed the hypothesis that the corrosion resistance of CoCr–keeper, PdAu–keeper and AuPt–keeper complexes might be different and that laser welding might contribute to these differences. To that end, oxalic acid solution etching and electrochemical evaluation tests were applied, followed by surface morphology observation, chemical elements analysis and Tafel polarization curve recording to investigate how several commonly used alloys couple with the same keeper in different methods of fabrication. We observed the extent of corrosion respectively, for each alloy, so as to explore their corrosion behaviour. After the measurement of the corrosive states of different alloys and keepers, we then discuss which alloy may provide the most benefit for preventing corrosion with respect to both alloy and keeper.

MATERIALS AND METHODS
Sample preparation
Fifty-two keepers (4.0-mm diameter, 0.8-mm thickness, SUS444) from a commercially-produced dental magnetic attachment system (Magfit DX800; Aichi Steel Works, Tokyo, Japan) and three cast alloys were used in this study. There were 24 keepers in both the cast and laser-welded dowel-keeper groups that were divided equally into three subgroups for the three alloys. The remaining 4 keepers were left freestanding and served as a control group. Another control group consisted of 4 castings of each alloy without any keepers.

The cast and laser-welded dowel-keeper groups had some of the same fabrication processes for wax pattern of a dowel and coping, similar to a previous report.[13] Briefly, the keeper was first placed in the centre of a stainless steel mould (10-mm inner-diameter, 2.0-mm height). The remaining space was then filled with fusing wax (casting wax; Nissin Dental Products, Kyoto, Japan) by the wax-melting method (Figure 1a), and a sprue was fused at the bottom edge of the wax pattern. After that, however, in the cast dowel-keeper group, wax pattern-embedded keepers were cast with CoCr cast alloy (Type Knd/cw-cc; Knd Material, Chengdu, China), PdAu cast alloy (containing 23.35% Ag and 10% In; Type Argelite. 61+3; Argen, San Diego, CA, USA) and AuPt cast alloy (Type Alfa ceramic 90; All Dental, Stockholm, Switzerland), respectively, to produce the cast keeper complexes. In the laser-welded dowel-keeper group, keepers were removed from wax patterns to leave a concave after the wax-melting. After investment casting, the keepers were welded into the reserved concave of the specimen surface in argon atmosphere[13,27–28] by the semi-automatic micro spot welder (Primotec phaser; Primotec, Pforzheim, Germany).

A copper wire (1.0-mm diameter, 150-mm length) was securely welded at the middle of the specimen bottom (Figure 1b). The resistance between them verified to be 0 Ω by a universal power meter set 200 Ω; otherwise, they were re-welded. The copper wire was bent into a right angle and passed through the lateral hole (6.0-mm diameter) of a hollow cylinder made by a 5-mL disposable syringe. We then filled the self-curing resin onto the back of specimen situated in the centre of cylinder until reaching the hemline of the hole. After

completely hardening, the resin was re-poured into the cylinder while a glass tube (6.0-mm diameter, 100-mm length) penetrated the hole with the remaining copper wire (Figure 1b). Next, other end of the tube was sealed with resin and checked for cracks between the specimen and the curing resin under optical microscope.

The surfaces of the samples were polished using waterproof abrasive paper (240#-1200#, gradually; Shanghai Grinding Wheels Plant, Shanghai, China) by metallographic grinding and polishing machine (1 000 r·min^{-1}, 60 s, Type Labopol-6; Struers, Ballerup, Denmark) and cleaned ultrasonically (40 KHz) for 10 min with dehydrated alcohol. Also, it was ensured that the surfaces were smooth and without excessive scarification under an optical microscope.

Oxalic acid solution etching test and analysis standard
The prepared samples were placed in a 10% oxalic acid solution in a stainless steel cup. A two-way voltage and current-stabilized power supply (RXN-1520D) was applied. The sample surface was placed near the anodic electrode, and the cup was placed near the cathodic electrode; currency density of 1 A·cm^{-2} was applied, etching for 60 s. Thereafter, samples were cleaned with distilled water and dried for surface morphology observation under an inversion metallographic microscope (Nikon Epiphot type 200).

In addition, before and after 10% oxalic acid solution etching, scanning electron microscope (SEM; Inspect F50; FEI, Hillsboro, OR, USA) and chemical elements analysis by Energy-dispersive spectroscopy (EDS; Type INCA Penta FET×3; Oxford, Oxfordshire, UK) were performed so as to comprehend the changes of chemical elements on the surfaces of the samples.

Electrochemical test and analysis standard
The fresh artificial saliva for Tafel polarization curve recording contained 6.84 mmol·L^{-1} NaCl, 5.37 mmol·L^{-1} KCl, 5.41 mmol·L^{-1} CaCl$_2$·2H$_2$O, 5 mmol·L^{-1} NaH$_2$PO$_4$·2H$_2$O, 16.65 mmol·L^{-1} Urea and 0.02 mmol·L^{-1} Na$_2$S·9H$_2$O and (pH = 6.8, ISO10271 standard). A prepared sample was placed at the study electrode in a beaker with 500 mL fresh artificial saliva. The saturated calomel electrode acted as the reference electrode[23,29] placed in the middle between the study electrode and the auxiliary electrode made by graphite electrode so as to form a standard three-electrode system. Electrodes were kept in the fixed place, each of which was connected to the potentiostat (Princeton Applied Research type 273A; AMETEK, Berwyn, IL, USA).

The open circuit potential-time curve (E_{ocp}–t current) of the study electrode immersed in electrolyte for 2 h without any applied voltage was recorded.[29] The constant potential rectifier set at E_{ocp}-300 mV of the initial scan potential scanned the study electrode by the rate of 1 mV·s^{-1} to the terminal potential of 1.1 V. The computer plotted the Tafel polarization curve according to the record data and obtained the logI_{corr} and E_{corr}.

In addition, pictures were taken of each sample surface morphology under inversion metallographic microscope after the electrochemical test.

Data analysis
The corrosion rate (v_{corr}) of each sample was calculated according to the formula:

$$v_{corr} = 0.163 \times A \times I_{corr} \times 10/d$$

in which A represented the average molecular weight of materials, I_{corr} represented free-corrosion current density and d represented the average density of materials, which were calculated online with the relevant formula on basis of the density and area of the keeper and alloys. Moreover, the evaluation standard was such that $v_{corr} < 0.01$ mm·A^{-1} suggested complete corrosion resistance, $v_{corr} <$
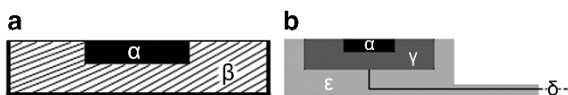
Figure 1 Model of sample preparation. (a) Fabrication of wax pattern (α, keeper; β, casting wax). (b) Connection with copper wire and resin embedding (γ, alloy casting; δ, copper wire; ε, self-curing resin).

$0.1 \text{ mm} \cdot \text{A}^{-1}$ suggested some corrosion resistance and $v_{corr} > 0.1 \text{ mm} \cdot \text{A}^{-1}$ suggested non-resistant corrosion.

Whenever possible, data are expressed as the mean ± standard error of mean. Statistical analyses were performed by the Origin 8.0 software and plot to the fitting curve. SPSS 18.0 software was applied for Mann–Whitney analysis and Kruskal–Wallis test. A value of $P < 0.05$ was considered significant.

RESULTS

Observation of sample surface morphology after oxalic acid solution etching

The alloy surfaces of the cast CoCr–keeper and laser-welded CoCr–keeper, giving rise to a large amount of metal oxide after 10% oxalic acid solution etching test, still retained a layer of insoluble oxide although most had washed away. The keeper of cast CoCr–keeper also developed thin attachments while the laser-welded CoCr–keeper did not. Whether casting or laser-welding for PdAu, the surface remained smooth except for some mist-like attachments observed on the keeper area closing of the sprue. However, the surface of the AuPt alloy generated a passivation layer without any depositions.

The results of observation under inversion metallographic microscope after 10% oxalic acid solution etching test were such that grain boundaries only appeared on the keepers of cast CoCr–keeper rather than the other five keeper complexes.

In the cast CoCr–keeper group, the keeper not only developed obvious grain boundaries but massive pitting corrosion that also occurred in the fusion zone and the alloy area only with oxydate (Figure 2a). The keeper of the laser-welded CoCr–keeper developed a few corrosion spots (Figure 2b) without visible grain boundaries, and the surface of the alloy had deep corrosion pits sedimentated with oxydate of a reticular structure.

Scattered corrosion holes and spots appeared on the keepers without grain boundaries in the cast PdAu–keeper group. In addition, the keeper surface closing of the sprue showed oxide deposition, but the alloy area showed almost no grain boundaries or large corrosion spots except for some corrosion holes in the alloy and fusion zone (Figure 2c). The surface features of the keeper in the laser-welded PdAu–keeper were equivalent to that of cast PdAu–keeper, and the fusion zone of the former exhibited serious corrosion pits and spots (Figure 2d).

Similarly, we failed to see intergranular corrosion in the cast AuPt–keeper's keeper even though it showed some scattered corrosion holes similar to the laser-welded AuPt–keeper. The fusion region formed a corrosion band in addition to the AuPt alloy being absent of obvious corrosion pits (Figure 2e). Corrosion pits developed on the laser-welding seam instead of the AuPt alloy area in the laser-welded AuPt–keeper group (Figure 2f).

Results of SEM and chemical elements analysis before and after oxalic acid solution etching test

With distinctive surface morphology before corrosion under SEM (Figure 3a), the fusion zone of cast CoCr–keeper has been demonstrated to be a Cr-rich oxide zone with Fe and Co released mainly from this area (Figure 4a) after the chemical elements analysis. Although the keeper area exhibited coarse lattice with many corrosion holes and a fusion area with an uneven corrosion band (Figure 3b), it also released a mass of Fe and Co after corrosion (Figure 4b). Unlike the cast CoCr–keeper with an oxidation zone before corrosion, the welding area of the laser-welded CoCr–keeper presented smooth convergence (Figure 3c) and both sides of the alloy kept their original structure after burnishing. The areas of Co, Fe and Cr coexisted at 0.3–0.5-mm wide in the welding area, demonstrating that the laser-welding resulted in the re-distribution of metal elements in the fusion zone (Figure 4c). Obvious corrosion bands and attached oxide were observed in the fusion zone of the laser-welded CoCr–keeper (Figure 3d) after corrosion. Compared with the results before corrosion, chemical elements analysis revealed that Co, Fe and Cr all were seriously reduced on the alloy side of the fusion zone and
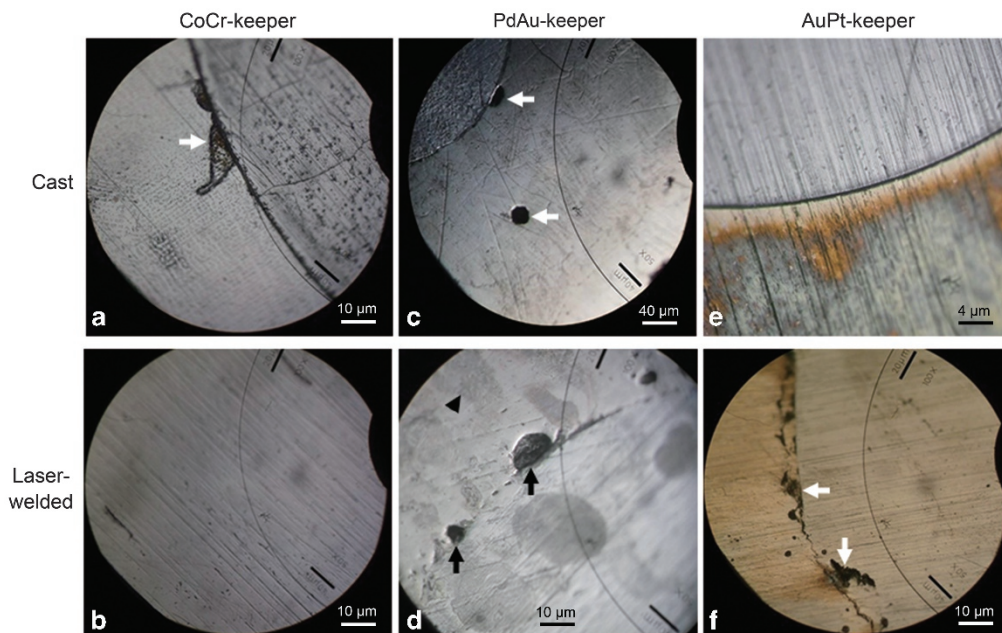
Figure 2 Observation of samples' surface morphology after oxalic acid solution etching. (**a**, Arrow, x200) Corrosion pits that are shallow concaves in the fusion zone. (**b**, x200) Only some scattered corrosion spots; sections with some outstanding features but no obvious defects existing on the keeper surface. (**c**, **d**) Corrosion holes that are deep hollows with massive defects (**c**, arrows, x50) and pits (**d**, arrows, x200) in the fusion zone and alloy area, along with flaky corrosion spots (**d**, arrowhead). (**e**, x500) A corrosion band formed in the fusion zone. (**f**, Arrows, x200) Corrosion pits occurred at the welding seam.

CoCr-keeper

Cast   Laser-welded

Cast PdAu-keeper
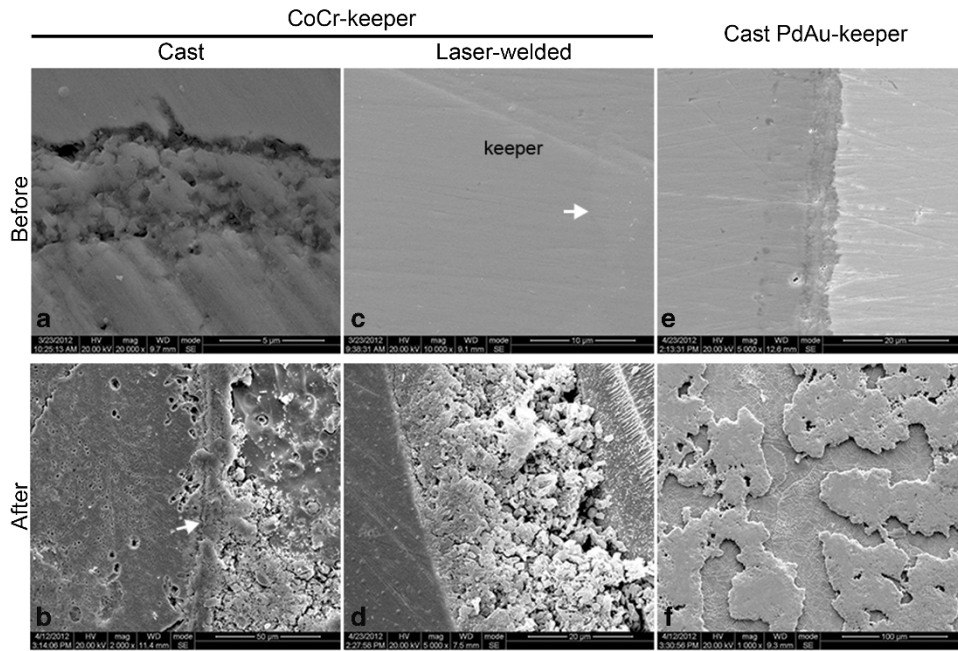
Figure 3 SEM observation before and after oxalic acid solution etching. (**a**, x20 000; **e**, x5 000) Before corrosion: the fusion area exhibited uneven surface after polishing. (**b**, Arrow, x2 000) After corrosion: a corrosion band appeared in fusion zone. (**c**, Arrow, x10 000) Before corrosion: a smooth surface in the welding area. (**d**, x5 000) After corrosion: the integrity of fusion zone was destroyed and a corrosion band formed. (**f**, x1 000) After corrosion: oxide deposition and fine grain boundaries on the keeper surface closing to the sprue. SEM, scanning electron microscope.

oxide was produced after corrosion, but the Fe and Cr of the keeper side remained unchanged (Figure 4d).

We next observed the surface features of the cast PdAu–keeper under SEM and analysed chemical elements changes before and after corrosion. The fusion zone showed barely any obvious oxide zone and had an uneven exterior despite polishing before corrosion (Figure 3e), and the keeper side gave rise to a none-Fe and Cr-rich band ~ 15-µm wide (Figure 4e). After corrosion, the keeper area adjacent to the sprue deposited some oxide, and no obvious corrosion was found in the grain boundaries on the surface (Figure 3f). The distal side had no oxide or grain boundaries. Chemical elements analysis indicated that corrosion pits appeared in the Cr-rich area after corrosion (Figure 4f). However, due to the re-distribution of metal elements, the fusion zone of the laser-welded PdAu–keeper formed an area with Pd, Ag, Fe and Cr coexisting at ~ 30-µm wide before corrosion (Figure 4g). Interestingly, no elements changed in the welding spot area despite corrosion spots that formed after corrosion (Figure 4h), but the chemical elements analysis of edges of serious local corrosion holes showed that Fe and Cr reduced significantly as compared with that before corrosion (Table 1).

A chemical elements analysis was also performed for the AuPt–keeper complex to detect the changes of distribution for various elements before and after corrosion. Similarly, a Fe-poor and Cr-rich band ~ 3–5-µm wide was generated on the keeper side of the fusion zone of the cast AuPt–keeper before corrosion, but no oxygen element was detected (Figure 4i). After corrosion, a corrosion groove ~ 3–5-µm wide appeared in the fusion zone with Fe obviously reduced (Figure 4j). However, a Cr-rich band had not formed on the edge of the keeper adjacent to the fusion zone of the laser-welded AuPt–keeper that had a smooth connection before corrosion (Figure 4k). The welding seam became deeper and clearer after corrosion, and the keeper side developed corrosion pits along with a significant decrease in Fe and Cr (Figure 4l).

Table 1 Chemical elements' changes in the fusion zone of the laser-welded PdAu-keeper before and after corrosion

Element	Mass percentage/%	
	Before corrosion	After corrosion
Cr	14.28	8.54
Fe	51.99	6.29
Pd	27.58	31.74
Ag	6.15	15.43
C	–	19.99
O	–	14.43

Observation of samples' surface morphology after electrochemical test

Scattered corrosion spots and shallow concaves were found on the surface of CoCr castings (Figure 5g). In the cast CoCr–keeper group, each area had different surface morphology; the CoCr alloy area exhibited scattered corrosion spots and shallow concaves and the keeper produced many fine oxidation spots, but visible corrosion pits appeared in the fusion zone (Figure 5a). In contrast, no obvious corrosion pits or oxidation spots appeared in the fusion zone or keeper in the laser-welded CoCr–keeper group (Figure 5b), although scattered corrosion spots and holes existed on the CoCr alloy surface.

Only scattered corrosion spots were observed on PdAu castings after electrochemical test (Figure 5h). In the cast PdAu–keeper group, the fusion zone and its nearby keeper area showed serious corrosion banding (Figure 5c) or pits. However, the keeper central area and the edge of the PdAu alloy only exhibited corrosion spots or holes. Similarly, in the laser-welded PdAu–keeper group, obvious corrosion pits had appeared in the fusion zone (Figure 5d), and its two sides and
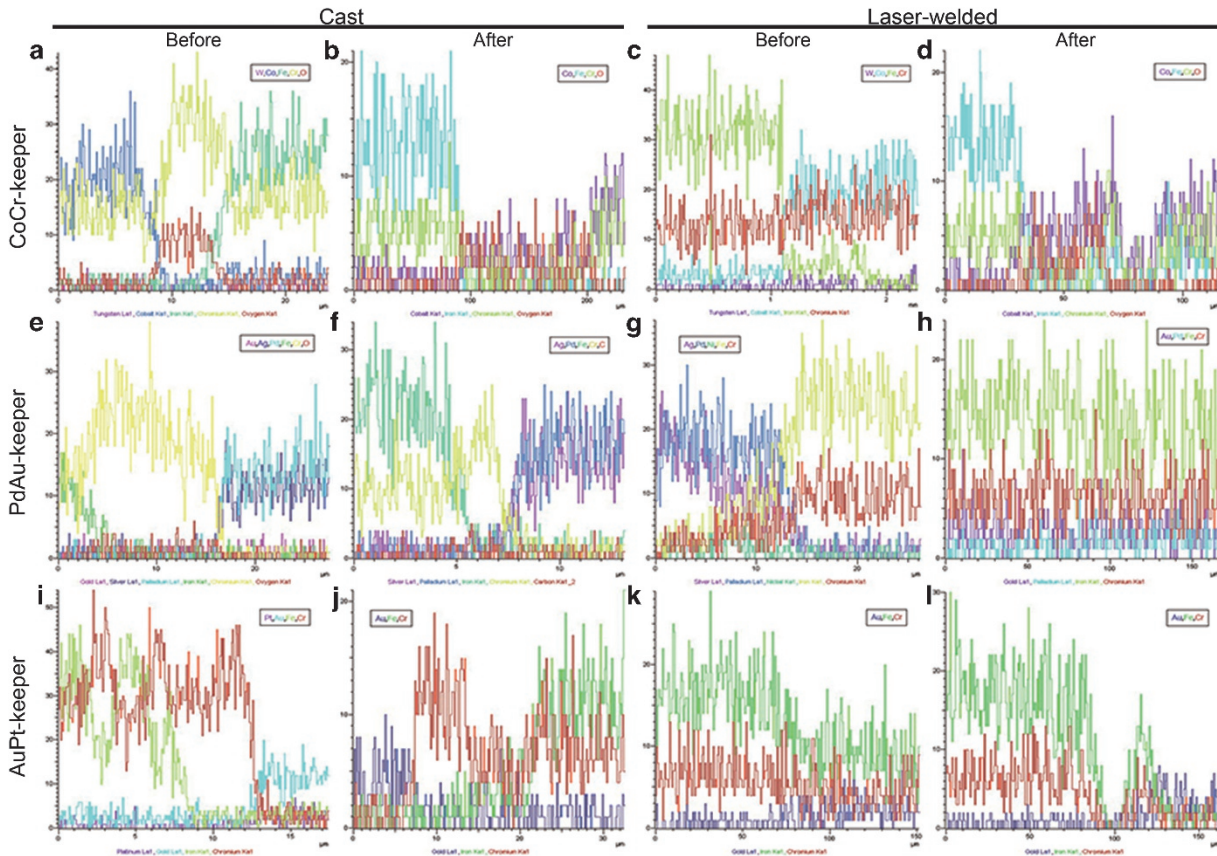
Figure 4 Elements analysis charts of the fusion zone before and after oxalic acid solution etching. (**a**) Before corrosion: a Cr-rich band formed. (**b**) After corrosion: Fe and Co elements decreased sharply. (**c**) Before corrosion: a Co, Cr and Fe coexisting area appeared. (**d**) After corrosion: Co, Cr and Fe elements obviously reduced. (**e**) Before corrosion: a none-Fe and Cr-rich band formed. (**f**) After corrosion: Fe element increased. (**g**) Before corrosion: a Pd, Ag, Fe and Cr coexisting band formed. (**h**) After corrosion: no elements obviously changed in the welding spot area. (**i**) Before corrosion: a Fe-poor and Cr-rich band formed. (**j**) After corrosion: Fe element obviously decreased. (**k**) Before corrosion: no Cr-rich band found. (**l**) After corrosion: Fe and Cr elements reduced sharply.

the surface morphology of the centre of the keeper and the edges of the PdAu alloy resembled that of the cast PdAu–keeper group.

Scattered corrosion spots were present on the AuPt castings (Figure 5i) as well as the PdAu castings. The keeper and AuPt alloy area were absent of corrosion holes in the cast AuPt–keeper group, and the fusion zone remained smooth without corrosion (Figure 5e). In the laser-welded AuPt–keeper group, corrosion pits were observed in the welding seam (Figure 5f), and pitting corrosion on the keeper. The AuPt alloy still maintained a complete surface.

Comparison of corrosion resistance of keeper complexes with the three cast and laser-welded alloys

Multiple comparisons among the E_{corr} values of the CoCr castings, PdAu castings, AuPt castings and keepers (Figure 6a) with Mann–Whitney test indicated statistically significant differences existed among them based on a significance of $P < 0.05$, and E_{corr} (CoCr castings) $< E_{corr}$ (keeper) $< E_{corr}$ (PdAu castings) $< E_{corr}$ (AuPt castings). Figure 6 also illustrates that the characteristics of the CoCr castings and keepers were completely corrosion-resistant due to the fact that both v_{corr} values were < 0.01 mm·A^{-1}. However, because the v_{corr} value fell between 0.01 and 0.1 mm·A^{-1}, PdAu castings and AuPt castings were corrosion-resistant alloys despite the fact that v_{corr} (AuPt castings) $< v_{corr}$ (PdAu castings; Figure 7b).

Multiple comparisons were also performed on the E_{corr} values of the cast keeper complexes including the cast CoCr–keeper, cast PdAu–keeper and cast AuPt–keeper to investigate statistically significant differences ($P < 0.05$), and E_{corr} (cast CoCr–keeper) $< E_{corr}$ (cast PdAu–keeper) $< E_{corr}$ (cast AuPt–keeper). Because v_{corr} was between 0.01 and 0.1 mm·A^{-1} for each of them, the three cast keeper complexes were all corrosion-resistant. Pitting potential (E_p) of the cast AuPt–keeper closing to the keeper's exceeded that of the cast CoCr–keeper and the cast PdAu–keeper, which were more similar (Figure 6d). However, the increase of current density in the cast CoCr–keeper was significantly more inferior to the cast PdAu–keeper and cast AuPt–keeper (Figure 7c).

Statistically significant differences ($P < 0.05$) were also found in multiple comparisons by Mann–Whitney test in the laser-welded CoCr–keeper, laser-welded PdAu–keeper and laser-welded AuPt–keeper according to each E_{corr} value from Figure 6a, and E_{corr} (laser-welded CoCr–keeper) $< E_{corr}$ (laser-welded PdAu–keeper) $< E_{corr}$ (laser-welded AuPt–keeper). Also, v_{corr} of the three laser-welded keeper complexes revealed them to be corrosion-resistant. Figure 7d showed E_p (laser-welded PdAu–keeper) $< E_p$ (laser-welded AuPt–keeper) $< E_p$ (laser-welded CoCr–keeper).

The results of Kruskal–Wallis and Mann–Whiney tests ($P < 0.05$) among all samples including alloy castings and keepers indicated: E_{corr} (cast CoCr–keeper) $< E_{corr}$ (laser-welded CoCr–keeper); E_{corr}
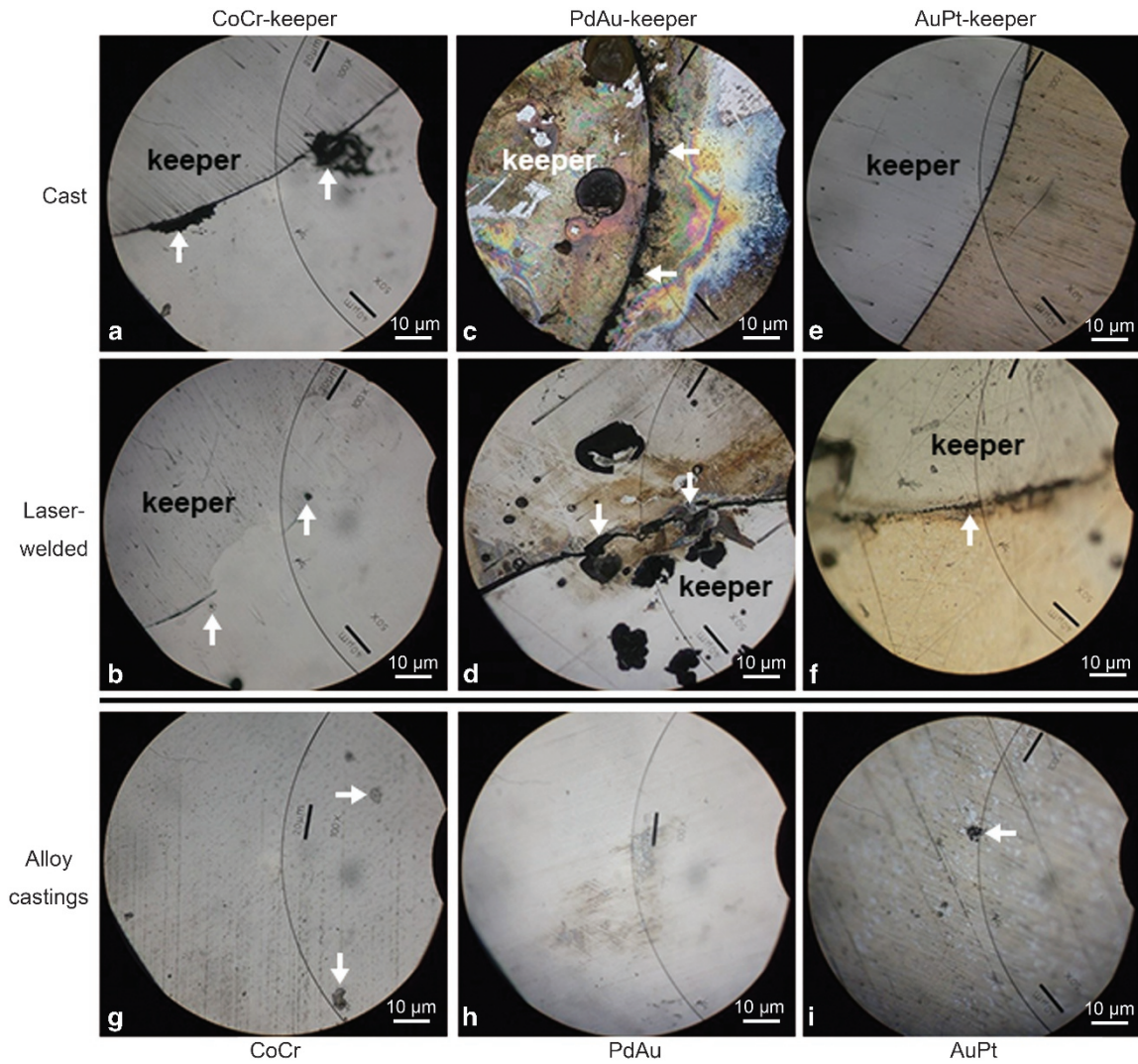
Figure 5 **Observation of samples' surface morphology after electrochemical testing**. (**a**, **d**, **f**, Arrows, x200) Corrosion pits in fusion zone. (**b**, x200) No obvious corrosion pits except for a few holes found (arrows) in fusion zone. (**c**, Arrows, x200) A corrosion band formed in fusion zone. (**e**, x200) The fusion zone remained smooth. (**g–i**, Arrows, x200) Corrosion spots on the surface of alloy castings.
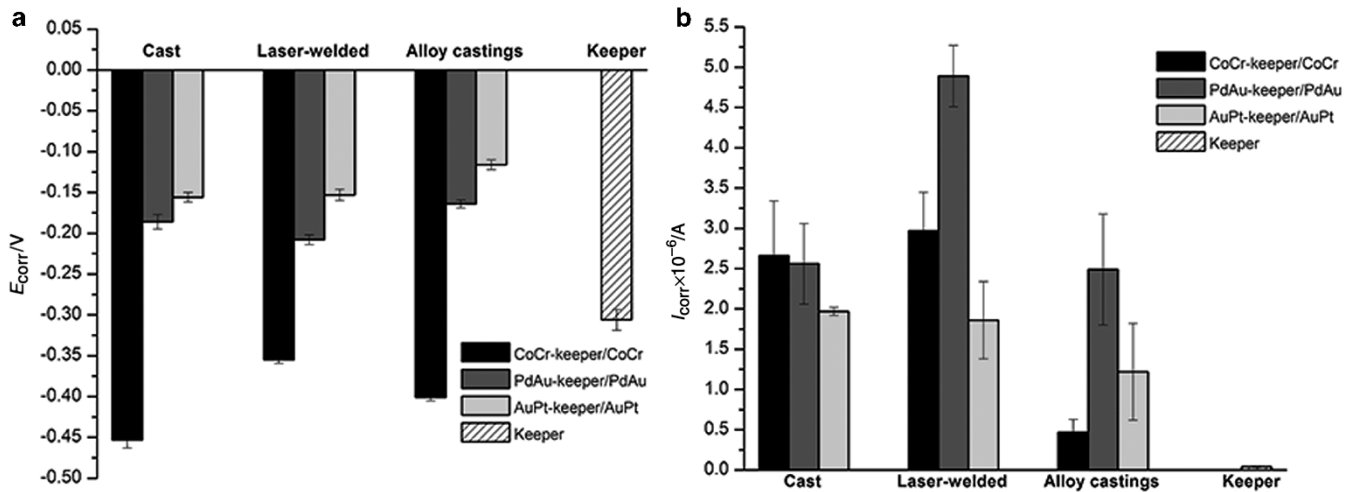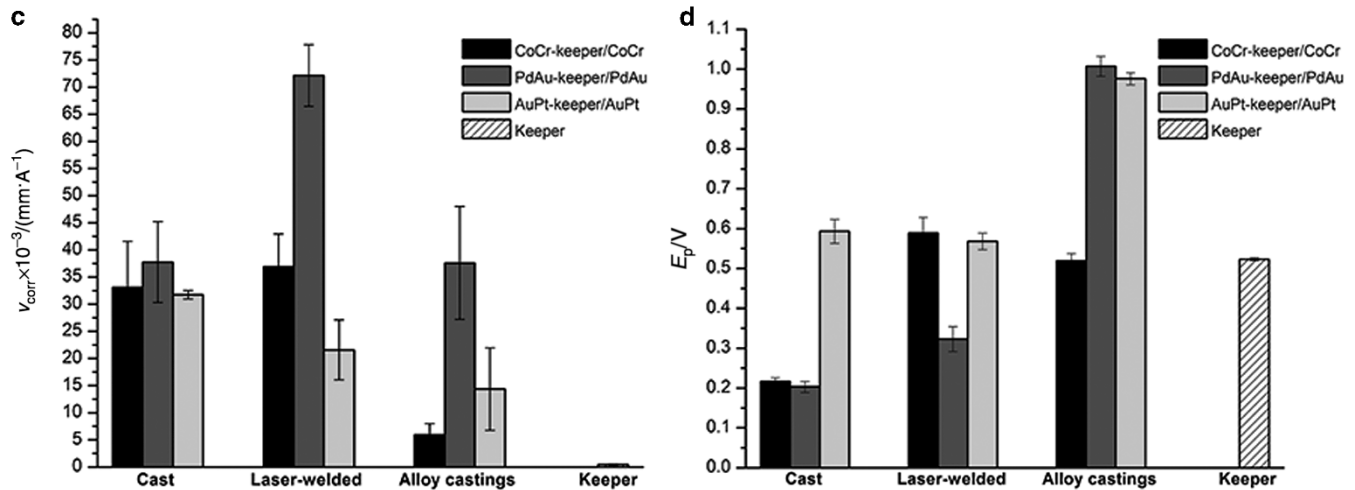
Figure 6 **Results of dynamic electrochemical test of samples**. Scanned potentiodynamic polarization of different samples and plotted Tafel polarization curve. (**a**) E_{corr}: free-corrosion potential, relative potential value when SCE acts as the reference electrode. (**b**) I_{corr}: free-corrosion current density. (**c**) v_{corr}: corrosion rate. (**d**) E_p: pitting potential appeared when the passivation film on the metal surface was destroyed. SCE, saturated calomel electrode.
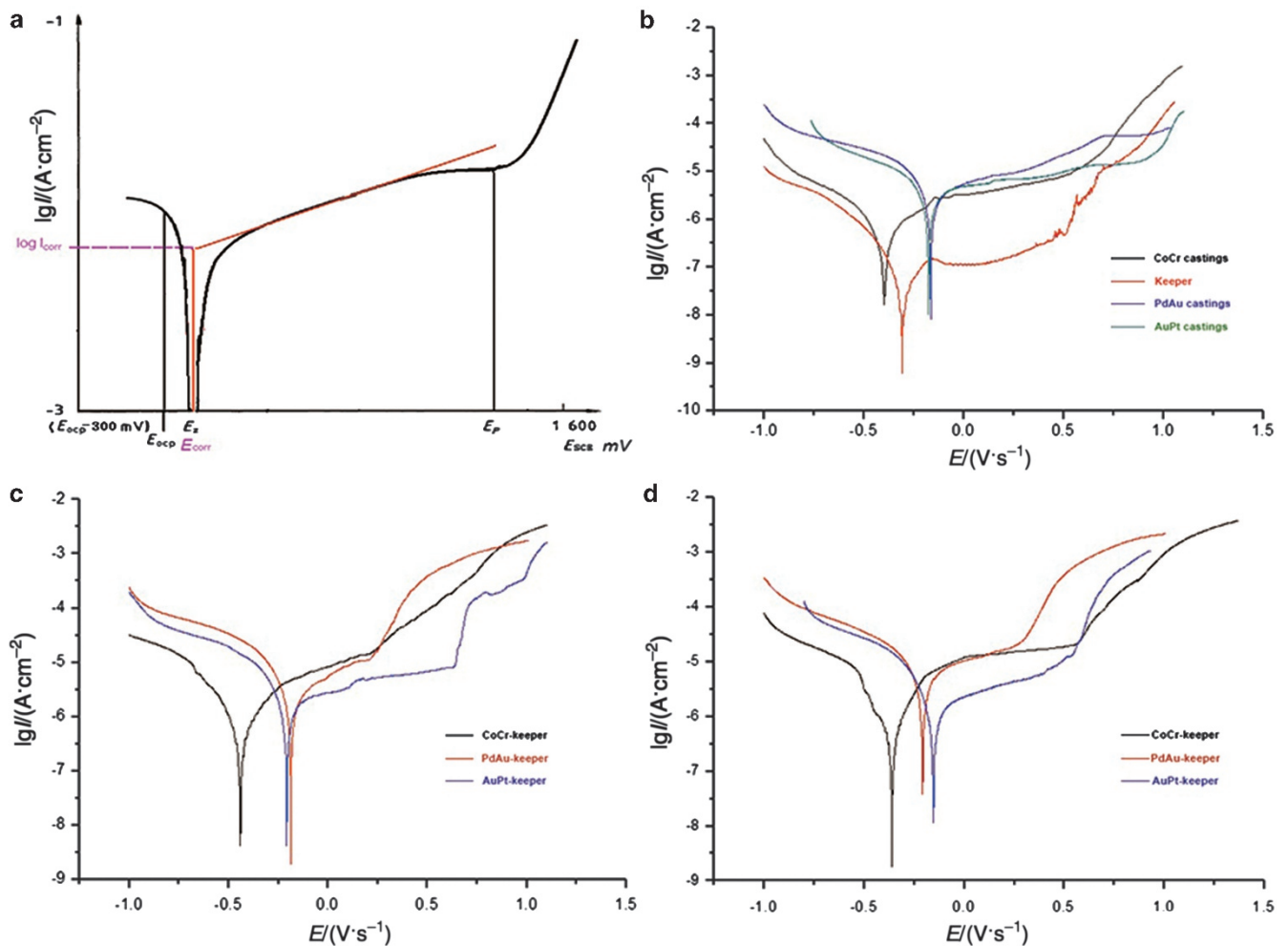
Figure 7 **Tafel curves of samples during electrochemical test.** (**a**) Typical Tafel polarization curve. (**b**) Tafel curves of the three alloy castings and keeper. (**c**) Tafel curves of cast keeper complexes. (**d**) Tafel curves of laser-welded keeper complexes.

(laser-welded PdAu–keeper) $<$ E_{corr} (cast PdAu–keeper); E_{corr} (cast AuPt–keeper) $=$ E_{corr} (laser-welded AuPt–keeper); E_p (cast CoCr–keeper) $<$ E_p (laser-welded CoCr–keeper); E_p (cast PdAu–keeper) $<$ E_p (laser-welded PdAu–keeper); and E_p (cast AuPt–keeper) $=$ E_p (laser-welded AuPt–keeper).

DISCUSSION

In this study, common chemical and electrochemical tests were applied to explore the corrosion behaviour of different keeper complexes. The chemical tests indicated that corrosion occurred when the oxidant in a non-electrolyte solution contacted metal, and the electrochemical tests showed that electronic exchange occurred between the metal and the electrolyte to form metal ions. There is no doubt that the electro-chemical corrosion is the primary and most serious type of corrosion in oral cavity because saliva contains 99.4% water and 0.6% of inorganic ions and organic compounds.[21] In this study, 10% oxalic acid solution, which is a weak acid that simulates the oral environment in a low pH condition, was applied in a chemical test to observe and analyse the changes of sample surface. The artificial saliva was prepared fresh as the electrolyte solution to simulate a neutral oral environment for electro-chemical testing according to ISO10271 standard.

One factor influencing the corrosion behaviour of the keeper complexes were the types of alloy used in this study, including CoCr, PdAu and AuPt. From the results above, it is not difficult to see that the fusion zone was the most and most easily corroded part of the complex; the Fe/Co and Fe/Cr elements were significantly reduced in the CoCr–keeper, PdAu–keeper and AuPt–keeper complexes after corrosion, respectively. The CoCr alloy area obviously gave rise to oxide attach-ment after the chemical test, but intergranular corrosion only appeared in the keeper area of the cast CoCr–keeper without oxide. Thus, it may be seen that CoCr alloy was the main corrosion object in the CoCr–keeper complex, meaning that the keeper acted as a cathode and CoCr alloy as an anode to form a galvanic corrosion that accelerated the anode corrosion when both were put in the same etching solution. We may conclude that CoCr alloy and the keeper adjacent to the fusion zone were corroded because the Fe and Co reduced what were main elements of keeper and the alloy, respectively. After chemical testing, oxides could not be found adhering to the surface of the fusion zone of the PdAu–keeper complex but did exist on the keeper area closing of the sprue. Thus, the keeper had proven to be the main corrosion area of the cast PdAu–keeper. The fusion zone was recognized as a composite area containing Cr, Fe, Pd, Ag and In elements. In and Fe easily lost electrons in order to be ions when contacted with Au, Pd, Ag of high potential, so that Fe reduced obviously in the fusion zone after corrosion. However, under metalloscope we observed that the PdAu–keeper complex displayed extremely serious corrosion to the alloy, keeper and the fusion zone after electrochemical testing. The situation could be construed as Ag with diverse redox states in different corrosion. The keeper of the AuPt–keeper complex always maintained a smooth surface without attachments in the chemical test. Metallo-scope and chemical elements analysis had suggested that a corrosion band formed on the edge of the keeper and that Fe and Cr reduced significantly. We speculate that Fe^{2+} was absent from keeper, and that Au and Pt constituted galvanic couples to form an oxide film containing Fe^{3+} on the AuPt alloy surface where trace amount of Fe was also detected by chemical element analysis.

Another factor influencing the corrosion behaviour were the cast and laser-welded fabrication methods for a keeper complex. This study has demonstrated that the E_{corr} and E_p values of the laser-welded CoCr–keeper were greater than that of cast CoCr–keeper, indicating that the passivated state of the cast CoCr–keeper could easily be

destroyed and its corrosion-resistance was inferior to that of the laser-welded CoCr–keeper. Recent studies have acknowledged that the surfaces of keeper cast made with nickel–chromium alloy or titanium gave rise to coarse grains, but no obvious changes appeared when cast with gold alloy.[13] However, the keeper surface, except the heat reaction zone, maintained its original metallographic structure after laser welding. With a metallographic structure of body-centered cubic, the keeper made of SUS444 was an α-Fe-based interstitial solid solution. In addition, the metallographic structure changed to face-centred cubic when α-Fe transformed into γ-Fe at 912 °C so as to form austenite. However, the original metallographic structure was destroyed when cooled due to segregation causing uneven distribution of elements to form residual austenite and bainite, which resulted in intergranular corrosion occurring easily. As is well-known, the samples of the cast CoCr–keeper would be preheated for 1 h at 90 °C, which is lower than CoCr alloy's melting temperature (1 350 °C–1 420 °C) before casting. However, laser welding applied for a short time to each sample caused α-Fe to remain unchanged, when made only at local high-temperature and cooled rapidly,[30] allowed so that the original metallographic structure stayed the same. Consequently, the corrosion-resistance of the laser-welded CoCr–keeper was superior to that of cast CoCr–keeper. Although the melting temperature of the PdAu alloy was 1 110–1 280 °C above the phase transition temperature of α-Fe, the effect of casting temperature on the keeper was inferior to CoCr alloy's because of the self-cooling that started after casting. Because of the welding defects that occurred in the laser-welding process such as the welding seams and concaves that brought about crevice corrosion, E_{corr} of the laser-welded PdAu–keeper was slightly lower than that of the cast PdAu–keeper. In contrast, the fact that E_p of the laser-welded PdAu–keeper was significantly higher than that of cast PdAu–keeper indicates that the casting process of the PdAu alloy had a certain impact on the keeper's metallographic structure, resulting in a passive film that was easily destroyed. Thus, improving the welding technology and quality could enhance self-corrosion resistance even though the self-corrosion trend of the laser-welded PdAu–keeper was only a little higher than that of cast PdAu–keeper. The preheating temperature of AuPt (780 °C) was far below the phase transition temperature of α-Fe, which had little effect on the keeper's metallographic structure despite a slightly higher melting temperature of the AuPt alloy (1 040–1 120 °C). Thus, no significant difference in either E_p or corrosion-resistance was found between the cast and laser-welded AuPt–keepers.

Whether cast or laser-welding, the fusion zone has been proved to be the most corrosion-prone area according to results from metallo-scope and SEM. In accordance with our results, Edmond *et al*.[31] observed that an unevenly banded joining seam was generated in the fusion zone after cast, finding that the oxide layer could be effectively prevented by reducing the pretreatment temperature during the casting process. However, this study has demonstrated a Fe-poor and Cr-rich band was detected on the edge of the keepers in the cast dowel-keeper group, and only the Cr-rich area of cast CoCr–keeper developed oxidation. Thus, the so-called oxide layer might be due to the re-arrangement of elements from the edges of the keepers during casting. However, there is no doubt that the Cr-rich band would be the most sensitive corrosion area in cast keeper complexes. With characteristics of rapid heating, fast cooling and short action time,[27–28,30] laser-welded keeper complexes had no Cr-rich band in the welding area and no changes of metallographic structure in the alloy area adjacent to leakage-welded seam. A continuous corrosion groove appeared only around the keeper of the laser-welded CoCr–keeper and others with some corrosion pits. However, the presence of a welding seam would give rise to crevice corrosion, influencing the

combination of the keeper and the alloy. Therefore, further study is necessary to develop the quality of laser welding.

CONCLUSION

According to the above results, we could summarize that the corrosion-resistance of the three alloy castings was such that AuPt > PdAu > CoCr. The edges of all keepers developed a Fe-poor and Cr-rich band that experienced accelerated corrosion when casting. In galvanic couples composed by keeper and different alloys, PdAu and AuPt alloys acting as the cathode were protected, but CoCr alloy as the anode was corroded, owing to its low free corrosion potential. Whether cast or laser-welded, the fusion zone was the most sensitive corrosion area. From the E_{corr} values among them, we could conclude that the corrosion resistance of cast AuPt–keeper was most optimal and cast CoCr–keeper was the worst. Similarly, an abundance of oxide and the E_{corr} value indicated that the corrosion resistance of laser-welded CoCr–keeper was the worst. However, the laser-welded CoCr–keeper could maintain the existence of a keeper surface passive and the original metallographic structure, revealing that its corrosion resistance is superior to the cast CoCr–keeper. The keeper area of the laser-welded PdAu–keeper also kept its original metallographic structure while the cast PdAu–keeper suffered the appearance of intergranular corrosion, illustrating that the former's anti-corrosion property was better. However, no obvious differences in corrosion-resistance were observed between the cast and laser-welded AuPt–keepers. On the basis of chemical elements analysis, the alloy and keeper areas adjacent to the fusion area had Fe- and Co-based corrosion that occurred in the CoCr–keeper complex, and the keeper area closing to the fusion zones of the PdAu- and AuPt–keeper complexes were the main corrosion sites where Fe reduced most and Cr followed.

This study provides a reference on selecting alloys for dowel-coping and appropriate fabrication methods for the keeper complex, thus helping to improve their corrosion-resistance and long-term effects.

1   Takahashi N, Takada Y, Okuno O. Galvanic corrosion between dental precious alloys and magnetic stainless steels used for dental magnetic attachments. *Dent Mater J* 2008; **27**(2): 237–242.

2   Riley MA, Walmsley AD, Harris IR. Magnets in prosthetic dentistry. *J Prosthet Dent* 2001; **86**(2): 137–142.

3   Cheng T, Sun G, Huo J *et al*. Patient satisfaction and masticatory efficiency of single implant-retained mandibular overdentures using the stud and magnetic attachments. *J Dent* 2012; **40**(11): 1018–1023.

4   Rubenstein JE. Attachments used for implant-supported facial prostheses: a survey of United States, Canadian, and Swedish centers. *J Prosthet Dent* 1995; **73**(3): 262–266.

5   Okuno O, Ishikawa S, Imuro FT *et al*. Development of sealed cup yoke type dental magnetic attachment. *Dent Mater J* 1991; **10**(2): 172–174.

6   Highton R, Caputo AA, Matyas J. Retentive and stress characteristics for a magnetically retained partial overdenture. *J Oral Rehabil* 1986; **13**(5): 443–450.

7   Sasaki H, Kinouchi Y, Tsutsui H *et al*. A magnetic attachment for overdentures. *J Prosthet Dent* 1984; **51**(4): 450–455.

8   Gillings BR. Magnetic retention for complete and partial overdentures. Part I. *J Prosthet Dent* 1981; **45**(5): 484–491.

9   Gillings BR. Magnetic retention for overdentures. Part II. *J Prosthet Dent* 1983; **49**(5): 607–618.

10 Mensor MC Jr. Magnetic retention of the overdenture and removable partial denture: a new attachment system. *CDS Rev* 1982; **75**(4): 20–23.

11 Endo K, Suzuki M, Ohno H. Corrosion characteristics of ferric and austenitic stainless steels for dental magnetic attachment. *Dent Mater J* 2000; **19**(1): 34–49.

12 Boeckler AF, Ehring C, Morton D *et al*. Corrosion of dental magnet attachments for removable prostheses on teeth and implants. *J Prosthodont* 2009; **18**(4): 301–308.

13 Chao Y, Du L, Yang L. Comparative study of the surface characteristics, microstructure, and magnetic retentive forces of laser-welded dowel-keepers and cast dowel-keepers for use with magnetic attachments. *J Prosthet Dent* 2005; **93**(5): 473–477.

14 Wataha JC. Biocompatibility of dental casting alloys: a review. *J Prosthet Dent* 2000; **83**(2): 223–234.

15 Wataha JC, Lockwood PE. Release of elements from dental casting alloys into cell-culture medium over 10 months. *Dent Mater* 1998; **14**(2): 158–163.

16 Gonda T, Yang TC, Maeda Y. Five-year multicenter study of magnetic attachments used for natural overdenture abutments. *J Oral Rehabil* 2013; **40**(4): 258–262.

17 Riley MA, Williams AJ, Speight JD *et al*. Investigations into the failure of dental magnets. *Int J Prosthodont* 1999; **12**(3): 249–254.

18 Thean HP, Khor SK, Loh PL. Viability of magnetic denture retainers: a 3-year case report. *Quintessence Int* 2001; **32**(7): 517–520.

19 Leem HW, Cho IH, Lee JH *et al*. A study on the changes in attractive force of magnetic attachments for overdenture. *J Adv Prosthodont* 2016; **8**(1): 9–15.

20 Akin H, Coskun ME, Topcuoglu T *et al*. Can laser welding stop corrosion of new generation magnetic attachment systems? *Mater Res Innov* 2013; **15**(1): 66–69.

21 Phillips RW. *Skinner's science of dental materials*, 8th edn. Philadelphia: WB Saunders. 1982, 290–301.

22 Takada Y, Okuno O. Reversing potentials and increasing amount of released ions with contact corrosion between stainless steels and Au-Ag-Pd alloys. *J Jpn Dent Mater* 1996; **15**(6): 525–531.

23 Iimuro FT, Yoneyama T, Okuno O. Corrosion of coupled metals in a dental magnetic attachment system. *Dent Mater J* 1993; **12**(2): 136–144.

24 Reclaru L, Lüthy H, Eschler PY *et al*. Corrosion behaviour of cobalt-chromium dental alloys doped with precious metals. *Biomaterials* 2005; **26**(21): 4358–4365.

25 Sarantopoulos DM, Beck KA, Holsen R *et al*. Corrosion of CoCr and NiCr dental alloys alloyed with palladium. *J Prosthet Dent* 2011; **105**(1): 35–43.

26 Takasusuki N, Ida Y, Hirose Y *et al*. *In vitro* corrosion of dental Au-based casting alloys in polyvinylpyrrolidone-iodine solution. *Dent Mater J* 2013; **32**(3): 390–397.

27 Wang RR, Welsch GE. Joining titanium materials with tungsten inert gas welding, laser welding, and infrared brazing. *J Prosthet Dent* 1995; **74**(5): 521–530.

28 Yamagishi T, Ito M, Fujimura Y. Mechanical properties of laser welds of titanium in dentistry by pulsed Nd:YAG laser apparatus. *J Prosthet Dent* 1993; **70**(3): 264–273.

29 Manaranche C, Hornberger H. A proposal for the classification of dental alloys according to their resistance to corrosion. *Dent Mater* 2007; **23**(11): 1428–1437.

30 Roggensack M, Walter MH, Böning KW. Studies on laser- and plasma-welded titanium. *Dent Mater* 1993; **9**(2): 104–107.

31 Pow EH, Chan KH, Luk HW *et al*. Effect of burn-out temperature on magnetic keepers in cast noble metal alloy posts. *J Prosthet Dent* 2009; **101**(1): 66–72.